

Accurate Inverter Error Compensation and Related Self-Commissioning Scheme in Sensorless Induction Motor Drives

Original

Accurate Inverter Error Compensation and Related Self-Commissioning Scheme in Sensorless Induction Motor Drives / Pellegrino, GIAN - MARIO LUIGI; Bojoi, IUSTIN RADU; Guglielmi, Paolo; Cupertino, F.. - In: IEEE TRANSACTIONS ON INDUSTRY APPLICATIONS. - ISSN 0093-9994. - STAMPA. - 46:5(2010), pp. 1970-1978. [10.1109/TIA.2010.2057395]

Availability:

This version is available at: 11583/2370888 since:

Publisher:

IEEE

Published

DOI:10.1109/TIA.2010.2057395

Terms of use:

This article is made available under terms and conditions as specified in the corresponding bibliographic description in the repository

Publisher copyright

(Article begins on next page)

Accurate Inverter Error Compensation and Related Self-Commissioning Scheme in Sensorless Induction Motor Drives

Gianmario Pellegrino, *Member, IEEE*, Radu Iustin Bojoi, *Member, IEEE*, Paolo Guglielmi, *Member, IEEE*, and Francesco Cupertino, *Member, IEEE*

Abstract—This paper presents a technique for accurately identifying and compensating the inverter nonlinear voltage errors that deteriorate the performance of sensorless field-oriented controlled drives at low speed. The inverter model is more accurate than the standard signum-based models that are common in the literature, and the self-identification method is based on the feedback signal of the closed-loop flux observer in dc current steady-state conditions. The inverter model can be identified directly by the digital controller at the drive startup with no extra measures other than the motor phase currents and dc-link voltage. After the commissioning session, the compensation does not require to be tuned furthermore and is robust against temperature detuning. The experimental results, presented here for a rotor-flux-oriented SFOC IM drive for home appliances, demonstrate the feasibility of the proposed solution.

Index Terms—Back-EMF integration stator voltage integration, closed loop flux observer, compensation, induction motor drives, inverter nonlinearity compensation, inverters, machine vector control, online identification, self-commissioning algorithm, sensorless field-oriented control, sensorless induction motor drives, stator model.

I. INTRODUCTION

THE DIFFUSION of sensorless control in ac motor drives is expanding for the well-known advantages in terms of cost and reliability. Dealing with induction motor (IM) drives, many types of Sensorless Field Oriented Control (SFOC) have been proposed in the literature for different motor sizes and applications [1]. The performance of such SFOC schemes relies on the accuracy of the flux estimation: if the flux is not estimated correctly, the field orientation is imprecise and the IM drive does not work properly. The solutions proposed in the literature to estimate the flux by means of electrical quantities only (voltage and current vectors \tilde{v}_s , \tilde{i}_s) are based on the stator model of the motor, which is the time integral of the back-EMF

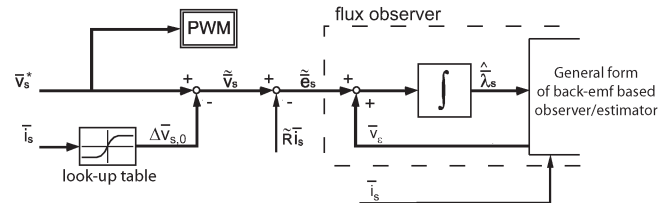


Fig. 1. Proposed inverter error compensation for SFOC IM drives with back-EMF-based flux estimation.

voltages. A feedback signal is needed to prevent the flux signal from drifting due to unavoidable offset at the integrator input; the feedback signal will be hereafter indicated as the *error voltage* signal \bar{v}_e of the flux estimator. In Fig. 1, the general form of a back-EMF-based flux observer for SFOC is reported, and the \bar{v}_e signal is put in evidence. Such a general form includes many flux estimation schemes: from simple low-pass filters [2] to more performing closed-loop observers like model-adaptive and/or sliding-mode observers [3]–[6]. Synchronous-frame observers, as the ones in [7], [8], are also included since the proposed identification is performed in dc conditions, where stationary and synchronous frames coincide. As outlined in Fig. 1, the estimated voltage vector \tilde{v}_s derived from the PWM reference voltage \tilde{v}_s^* is used for flux estimation instead of the measured voltage due to cost reasons and due to the difficulty of measuring pulse-width-modulated voltage signals. This hardware simplification introduces a voltage estimation error that is a nonlinear function of the motor current. The effects of such an error are evident at low speed and need to be properly compensated. Low speed is intended as the speed range where the back-EMF term is comparable or smaller than the resistive drop of the motor. In this condition, a good inverter error compensation becomes mandatory to obtain proper field orientation. Most of the compensation schemes in the literature rely on a simple and effective inverter model that consists of a series resistance (linear term) plus a threshold voltage (nonlinear term) on each motor phase that depends on the sign of the respective phase current, as formalized in [9]. Different techniques have been proposed, and some main examples are reported in [10]–[13].

Independent of the adopted scheme, the positive effect of the compensation depends on the correct tuning of the inverter model for any given power hardware. The signum-based model is very simple since it is described by two parameters only: the voltage threshold and a differential resistance. Datasheet-based and self-commissioning-based strategies are proposed by the

Manuscript received September 29, 2009; revised December 20, 2009 and January 27, 2010; accepted February 7, 2010. Date of publication July 26, 2010; date of current version September 17, 2010. Paper 2009-IDC-317.R2, presented at the 2009 IEEE Energy Conversion Congress and Exposition, San Jose, CA, September 20–24, and approved for publication in the IEEE TRANSACTIONS ON INDUSTRY APPLICATIONS by the Industrial Drives Committee of the IEEE Industry Applications Society.

G. Pellegrino, R. I. Bojoi, and P. Guglielmi are with the Politecnico di Torino, 10129 Turin, Italy (e-mail: gianmario.pellegrino@polito.it; radu.bojoi@polito.it; paolo.guglielmi@polito.it).

F. Cupertino is with the Politecnico di Bari, 70125 Bari, Italy (e-mail: cupertino@deemail.poliba.it).

Color versions of one or more of the figures in this paper are available online at <http://ieeexplore.ieee.org>.

Digital Object Identifier 10.1109/TIA.2010.2057395

referenced authors for tuning those two parameters, and they normally require extra processing and off-line computation to set the model parameters.

This paper introduces a more accurate compensation of the error introduced by the inverter: the nonlinear term is identified and represented by a modified signum function that is stored into a look-up-table (LUT). The LUT contains the actual values of the inverter nonlinear error around zero current, and performs a gradual and exact compensation that improves the flux estimation accuracy with respect to the signum function case. The LUT-based compensation is similar to the one recently proposed in [14], but the implementation here is more straightforward, and the identification procedure is very quick and does not need any further off-line processing. LUT compensation has been also proposed (but not implemented) in [15] for sensorless control with high-frequency signal injection. However, the method proposed here has not been tested with superimposed high-frequency signals so far, and this will be the scope of future works.

The LUT identification is performed by the digital controller at the drive startup. The information is provided by the flux observer error signal \bar{v}_e in dc steady-state conditions, as first reported in [16]. At zero frequency, in fact, the back-EMF is zero and the feedback signal equals the back-EMF estimation error. At the first drive startup, a proper sequence of current steps is set to identify the inverter error and then stored in the LUT. Each current step lasts 0.3 s, and the procedure takes about 15 s for the motor under test. It must be noted that the proposed method allows estimating the sum between the stator resistance and the dynamic resistance of the power switches.

The paper is organized as follows. In Section II, the back-EMF estimation issues and the inverter model are reviewed. In Section III, the identification principle based on the flux observer is also reviewed. Then, the LUT compensation is introduced and the self-commissioning procedure is described and tested. In Section IV, a comprehensive experimental validation of the proposed solution is given.

II. BACK-EMF ESTIMATION AT LOW SPEED

The stator-model-based estimation of the IM flux relies on the back-EMF time integral in stator coordinates (1). Regardless of which flux is used for field-orientation—stator flux as in (1) or rotor flux as in (2)—the accuracy of back-EMF estimation directly influences the field orientation and performance of the control

$$\hat{\lambda}_s = \int (\bar{v}_s^* - \tilde{R}_s \bar{i}_s) dt = \int \tilde{e}_s dt \quad (1)$$

where $\hat{\lambda}_s$ is the observed stator flux vector, \bar{v}_s^* is the reference voltage vector, \tilde{R}_s is the estimated stator resistance, \bar{i}_s is the measured currents vector, and \tilde{e}_s is the back-EMF estimate

$$\hat{\lambda}_r = k_r^{-1} \left\{ \hat{\lambda}_s - \sigma L_s \bar{i}_s \right\} = k_r^{-1} \left\{ \int \tilde{e}_s dt - \sigma L_s \bar{i}_s \right\} \quad (2)$$

where $\hat{\lambda}_r$ is the observed rotor flux vector; $k_r = L_m/L_r$ is the coupling factor of the rotor windings; L_m , L_s , L_r are, respectively, the mutual inductance between the stator and the

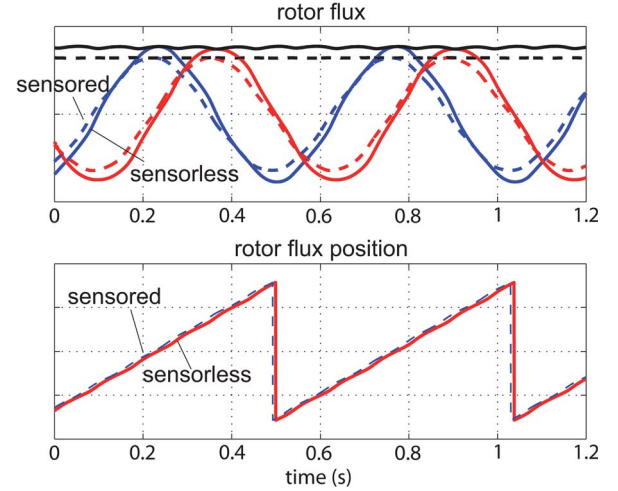


Fig. 2. Effect of uncompensated inverter error (100 r/min, experimental). Top: rotor flux obtained by sensed (dashed) and sensorless (continuous) observers. Bottom: estimated (continuous) and measured (dashed) rotor flux position. Scale factors: 0.5 Vs/div, 2 rad/div.

rotor windings, the stator inductance, and the rotor inductance; and $\sigma = 1 - L_m^2/(L_s L_r)$ is the total leakage factor.

A. Back-EMF Estimation Error

Dealing with back-EMF estimation, the inverter error and the stator resistance estimation error must be considered (3). The back-EMF estimation error follows accordingly (4)

$$\Delta \bar{v}_s = \bar{v}_s - \bar{v}_s^* \quad \Delta R_s = R_s - \tilde{R}_s \quad (3)$$

$$\Delta \bar{e}_s = \bar{e}_s - \tilde{e}_s = \Delta \bar{v}_s - \Delta R_s \bar{i}_s. \quad (4)$$

The inverter error $\Delta \bar{v}_s$ (5) is a nonlinear function of the motor phase currents, as described in [9]. It is given by the combined effects of turn-on dead-time and on-state voltage drops of the power switches (IGBTs and diodes) and includes a differential resistance term R_{on}

$$\Delta \bar{v}_s = \Delta \bar{v}_{s,0} - R_{on} \cdot \bar{i}_s. \quad (5)$$

The back-EMF error can finally be expressed as in

$$\Delta \bar{e}_s = \Delta \bar{v}_{s,0} - \Delta R \cdot \bar{i}_s \quad (6)$$

where the linear and nonlinear terms have been separated. $\Delta R = \Delta R_s + R_{on}$ stands for the estimation error of the whole series resistance (motor and inverter).

In current-controlled ac drives, the fast current controllers will output distorted reference voltage signals in order to obtain sinusoidal currents. When the distorted reference voltages are used for estimating the flux, an important error in field orientation occurs at low speed. An example of the position estimation error due to uncompensated inverter drop is given in Fig. 2 for the drive under test at 100 r/min. Moreover, the detuning of the stator resistance due to temperature variation (3) also contributes to the flux orientation error.

III. IDENTIFICATION AND COMPENSATION OF THE BACK-EMF ERROR

The general form of a back-EMF-based flux observer for SFOC control is shown in Fig. 1 and the feedback signal \bar{v}_e is put in evidence. The observer scheme adopted here is the one presented in [17], but the method is valid in general for most flux observers/estimators. The inverter error compensation is shown in Fig. 1, with the two compensation terms $\Delta\bar{v}_{s,0}$ and $\tilde{R} \cdot \bar{i}_s$ put in evidence.

The strategy for identifying the inverter error is based on the information given by \bar{v}_e in continuous current (dc) conditions. At zero frequency, the back-EMF is null. According to (4), the estimated back-EMF equals the overall estimation error in this case. Since the input of the back-EMF integrator is null in dc steady-state conditions, the exact estimation of the back-EMF error is

$$\tilde{e}_s + \bar{v}_e = 0 \Rightarrow \bar{v}_e = \Delta\bar{e}_s. \quad (7)$$

The identification principle is valid independent of the actual motor current value and it can be adopted for literally “plotting” the back-EMF error as a function of the motor current. In particular cases such as line filters or long cables, the identification principle (7) is still valid. In such cases, the voltage drop due to the series elements must be also considered in the back-EMF error model (6), but it is still true that it can be identified by means of the observer error. Dealing with long motor cables, the steep voltage transients mainly produce insulation stress and EMI problems and, eventually, voltage error. The remedies for such effects consist of filters, line terminators, or lowering the switching dynamics of the IGBTs through the gate commands and can be included in the identification. An example of back-EMF error identification is shown in Fig. 3(a), where a series of incremental current steps is applied to the motor under test. The current is injected along the α -axis. Each step lasts 0.2 s that corresponds to the settling time of the observer. The feedback signal $v_{e,\alpha}$ (trace 2) is negative since the injected current is positive. The final value that $v_{e,\alpha}$ assumes at the end of each time interval, after the observer transient is extinguished, is representative of the back-EMF error at that particular current level and it is stored in a table. The observer settling-time depends on the observer scheme and settings and the correct duration of dc current steps must be tuned according to the response of the $v_{e,\alpha}$ signal. The different curves shown in Fig. 3(b) (top) have been obtained by means of the procedure shown in Fig. 3(a) and they represent the back-EMF error as a function of the motor phase current. The discretization step along the current axis is 50 mA in this case. Two extreme situations are shown in Fig. 3(b): at first (dotted curve), the test has been carried out with the resistance compensation set to zero ($\tilde{R} = 0$) so that the back-EMF error includes the whole resistive term. In the second case (dashed line), the resistance was overcompensated during identification ($\tilde{R} > R$) so that the slope of the obtained curve is negative. Once the resistive part is eliminated from the two curves in Fig. 3(b), the nonlinear inverter error is identified and can be used for compensation in

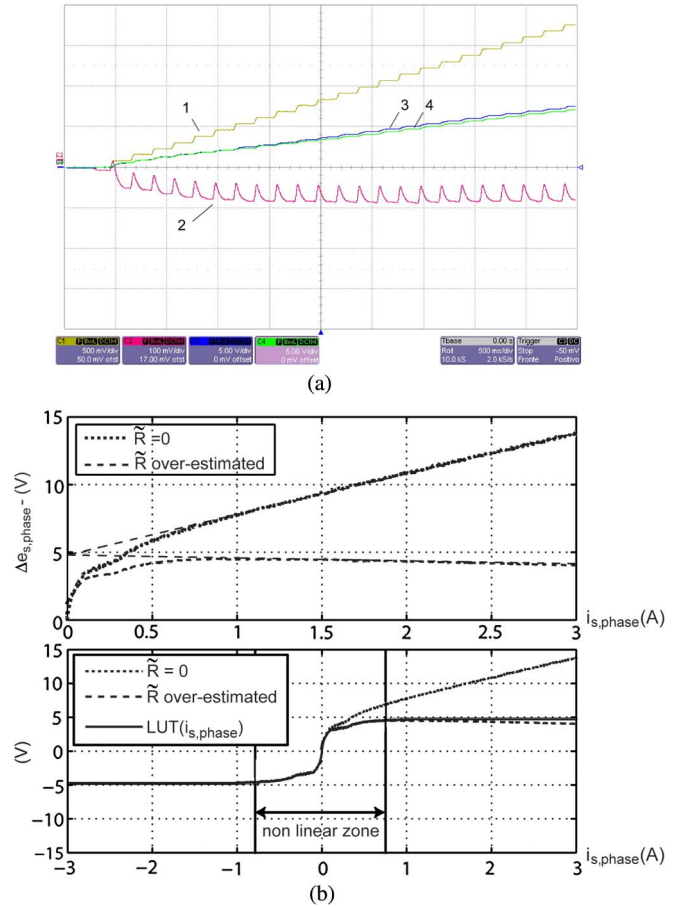


Fig. 3. Identification of the back-EMF estimation error by means of 0.1 A current steps along the α -axis. Scale factors of plot (a): 500 ms/div, 1: $i_{s,\alpha}^*$ (0.71 A/div), 2: $v_{e,\alpha}$ (4.5 V/div), 3 and 4: $\hat{\lambda}_{s,\alpha}$, $\hat{\lambda}_{r,\alpha}$ (0.24 Vs/div). (a) back-EMF error identification. (b) modified signum LUT.

the form of the smoothed signum function shown in Fig. 3(b) (bottom plot).

A. LUT Compensation Method

The back-EMF error compensation strategy shown in Fig. 1 is derived from the expression of the back-EMF error obtained in (6). As evidenced in Fig. 1, the linear and nonlinear terms are compensated separately. Once the back-EMF error is identified, the non-linear part of the inverter error $\Delta\bar{v}_{s,0}$ must be separated from the residual resistive term $\Delta R \cdot \bar{i}_s$. The nonlinear component consists of a smoothed signum function whose waveform is shown in Fig. 3(b) (bottom plot) for the drive under test. The current range where the curve is nonlinear is evidenced in the figure. In practical implementation, the nonlinear interval of that curve is stored in an LUT that is applied to the three-phase voltage components according to the signum of the respective phase currents. Since the flux observer is implemented in the bi-phase stationary frame α, β , the phase LUT must be rescaled by a factor 3/4 as in (8) according to the bi-phase to three-phase relationship described in detail in [16]. The α component of the inverter error in (8) is a reminder that the test has been performed with $\bar{i}_s = i_{s,\alpha} + j \cdot 0$

$$\Delta v_{s,0,phase}(i_{s,phase}) = 3/4 \cdot \Delta v_{s,0,\alpha}. \quad (8)$$

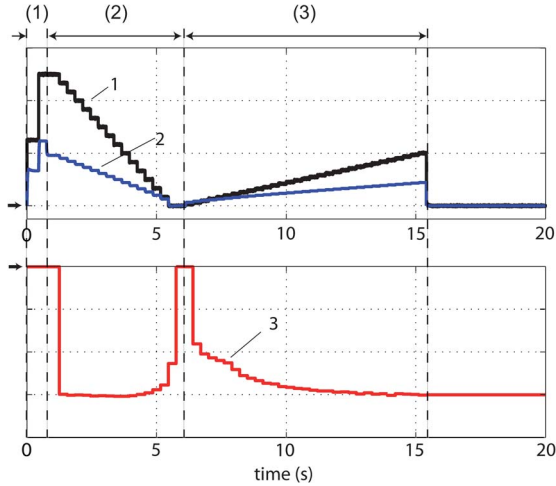


Fig. 4. Self-commissioning sequence, dead-time $1 \mu\text{s}$. 1: $i_{s,\alpha}$ (1 A/div), 2: $\lambda_{r,\alpha}$ (0.4 Vs/div), 3: $v_{\epsilon,\alpha}$ (2 V/div).

B. Self-Commissioning Algorithm

The self-commissioning algorithm is based on the principles stated in the previous section. As said, the current is supplied along the α -axis that is aligned to the motor phase a . The procedure takes about 15 s in the example drive (see the Appendix) and consists of three different stages, as shown in Fig. 4. With reference to the figure, note the following.

- 1) $t = 0 \div 0.75$ s. With both compensation terms off ($LUT = 0, \tilde{R} = 0$), two current steps are given (2.5 A and 5 A, duration 0.3 s each) and the total resistance is estimated by subtracting and scaling the two final values of the error signal $v_{\epsilon,\alpha}$;
- 2) $t = 0.75 \div 5.8$ s. With the resistance compensation enabled according to the resistance estimated at stage 1, a 16-step descending staircase (5 A to zero, delta step -0.25 A) is applied for individuating the current range where the error is nonlinear. The current level 1 A is found as the one where the feedback signal is 5% less than the $v_{\epsilon,\alpha}$ asymptotic value, stored with 5 A current;
- 3) $t = 5.8 \div 15.5$ s. A 32-step staircase is applied from zero to 2 A, which is twice the level found at stage 2 and a 32-element LUT is built. Each LUT point is calculated as the mean value of the v_{ϵ} signal over 16 samples for eliminating the effects of random noise.

The LUT obtained through the self-commissioning procedure is shown in Fig. 5 for the drive under test with the rated dead-time setting of $1 \mu\text{s}$ and also with a larger dead-time ($2 \mu\text{s}$) for the sake of comparison. The 32 points cover the phase current range $0 \div 2$ A. Linear interpolation is adopted in that range. For negative current values, the compensation sign is switched. For currents higher than 2 A, the final (maximum) value of the LUT is used. Stage 1 can be repeated in idle situations if the motor temperature varies significantly. Stages 2 and 3 can be performed just once, at the first drive startup, and do not need to be repeated. Stages 1 to 3 have been described with reference to an example case for the sake of simplicity, but the procedure can be extended to a general case. The current values at stage 1 (here 5 A and 2.5 A) must be chosen

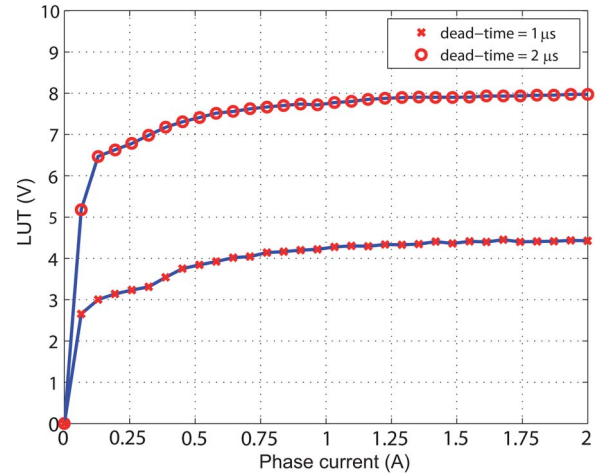


Fig. 5. 32-element LUT obtained by means of the self-commissioning session of Fig. 4: dead-time $1 \mu\text{s}$ and $2 \mu\text{s}$ cases are reported.

according to the maximum current rating of the inverter and must be high enough to ensure that they are both out of the nonlinear zone of the inverter voltage. In case of an improper choice of such current values, the resulting LUT would not be properly flat in the considered current range ($2.5 \text{ A} \div 5 \text{ A}$) and the identification should be started from the beginning with higher current values. Stage 2 is performed in 16 steps but lower values (e.g., 8) can be attempted for faster evaluation. Also in this case, the results are correct if the resulting LUT is properly flat around its maximum current value. Dealing with stage 3, a number of LUT points higher than 32 can give a better performance in case of a high dead-time, e.g., in low-voltage drives. About the duration of the dc current steps, 0.3 s has been chosen in the example according to the time-constant of the observer. As said, the signal $v_{\epsilon,\alpha}$ must be settled to its asymptotic value and the correct duration can be set by means of a preliminary test as the one in Fig. 3(a).

IV. EXPERIMENTAL RESULTS

The experimental tests have been performed using a 2-pole IM drive whose parameters are reported in the Appendix. The experimental setup is shown in Fig. 6: the motor under test is jointed with a torque-controlled synchronous motor used as a mechanical load. The motor is fed by the DMC1500 inverter board. Two different digital control platforms were used during the tests: 1) eZdsp F2808 employing the TMS320F2808 fixed-point DSP (Section IV-A); and 2) dSpace DS1103 board (Sections IV-B–D).

The floating-point dSPACE board is more convenient for developing the algorithm and, most of all, for capturing all the variables at once for the sake of fast and clear documentation of the experiments. On the other hand, the fixed-point implementation demonstrates the simplicity of the method and its feasibility in low-cost and industrial drives. In most of the presented tests, the same operating conditions will be compared for three different situations with respect to inverter error compensation: no inverter error compensation ($\Delta \bar{v}_{s,0} = 0$), signum-based compensation ($\Delta \bar{v}_{s,0} = k \cdot \text{sign}(\tilde{i}_s)$ [12], [16]), and the proposed LUT compensation.

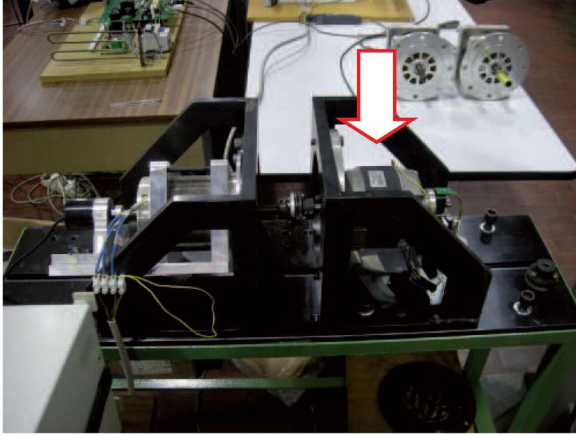


Fig. 6. Test rig. The arrow indicates the motor under test, coupled with a torque-controlled synchronous motor. Top right: other synchronous motors are available, e.g., the unskewed motor for loading with torque ripple. The power hardware is partially visible.

A. Open-Loop Current Control, 25 r/min

In Figs. 7 and 8, the induction motor is current-controlled at no load, i.e., a rotating stator current vector is applied to the machine, and three error compensation situations are compared. The magnitude of the current vector is the motor rated magnetizing current, while its angular speed corresponds to 25 r/min (0.41 Hz). At such low speed, the motor back-EMF is very small with respect to the stator resistance drop. Open-loop speed control ensures that the motor speed and load conditions are the same in all the tests, independent of the adopted compensation scheme because the flux-observer is not taking part in the drive control. In Fig. 7, the positive effect of both the types of compensation (b) and (c) is shown by the x - y plots in Fig. 7 since the trajectory of the estimated voltage is practically circular in both cases. The electrical speed is also well estimated in both cases, even if in Fig. 7(b), there is a residual distortion that does not appear in Fig. 7(c). Still, the radius of the reference voltage circles is different in cases (b) and (c), while the actual motor voltage is surely the same due to open-loop operation. A more detailed analysis of the compensation effect is obtained by evaluating the x - y trajectories of the estimated back-EMF instead of the voltages, as in Fig. 8. In this case, the difference between case (b) and case (c) is more evident: with the LUT compensation, the back-EMF signals are in quadrature with the phase current, as expected at no load, while with signum they are not.

B. Sensorless Control, 100 r/min, No Load

The motor is controlled using a rotor SFOC with speed control at 100 r/min and no load. The estimated back-EMF waveforms obtained with SFOC are shown in Fig. 9 and are similar to the ones registered in open loop. Still, the back-EMF obtained by the LUT compensation look smoother, but no phase orientation error is evidenced with signum compensation. However, at 100 r/min the difference between signum and LUT compensation is less evident than at 25 r/min, at least at no load.

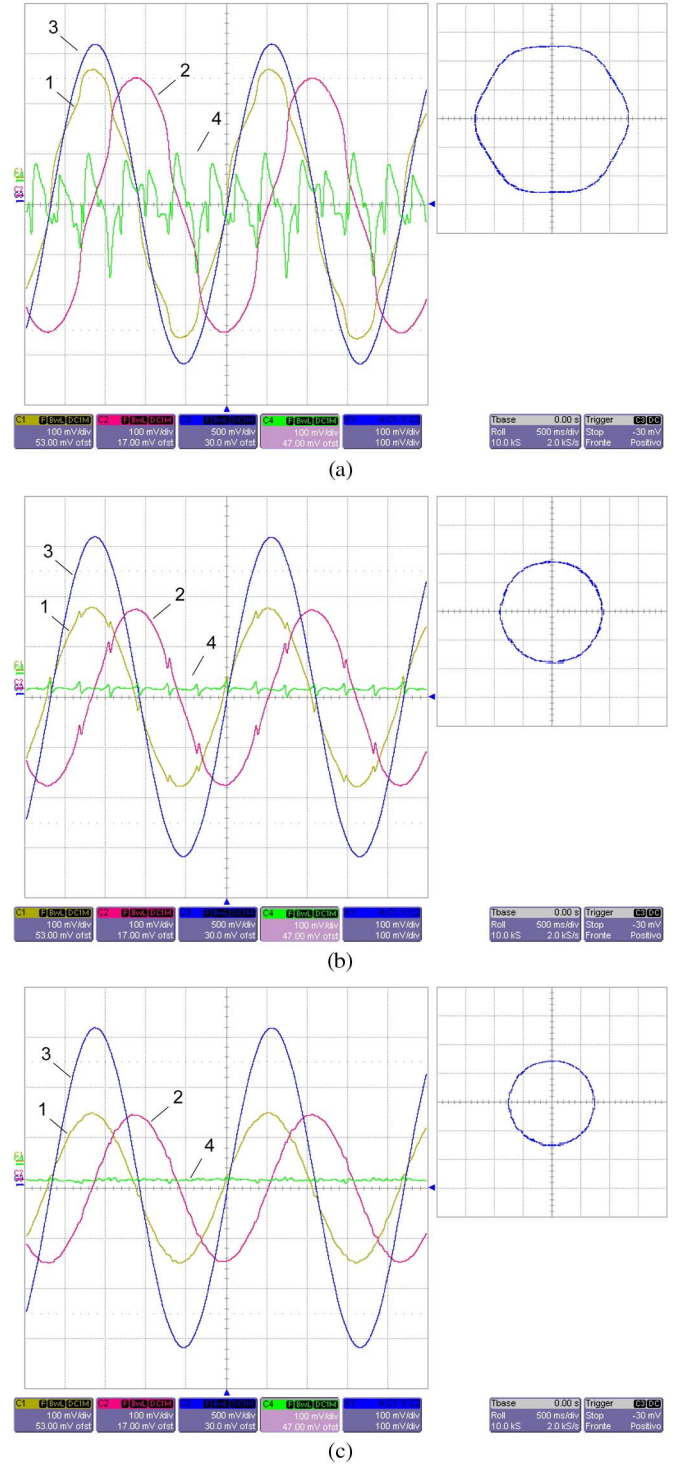


Fig. 7. Current control, open loop, no load, 25 r/min. Effect of the inverter error on the reference voltage signals and on the estimated electrical speed for different compensation situations. Scale factors: 500 ms/div, 1: $v_{s,\alpha}$ (4.5 V/div), 2: $v_{s,\beta}$ (4.5 V/div), 3: $i_{s,\alpha}$ (0.7 A/div), 4: ω_e (180 r/min/div). (a) compensation OFF. (b) signum compensation. (c) LUT compensation.

C. Sensorless Control, 100 r/min, With Step Load Transients

The motor is speed controlled using a rotor SFOC and step load transients are performed using the torque-controlled synchronous motor (Fig. 6). The loading motor has a skewed rotor and thus a low torque ripple.

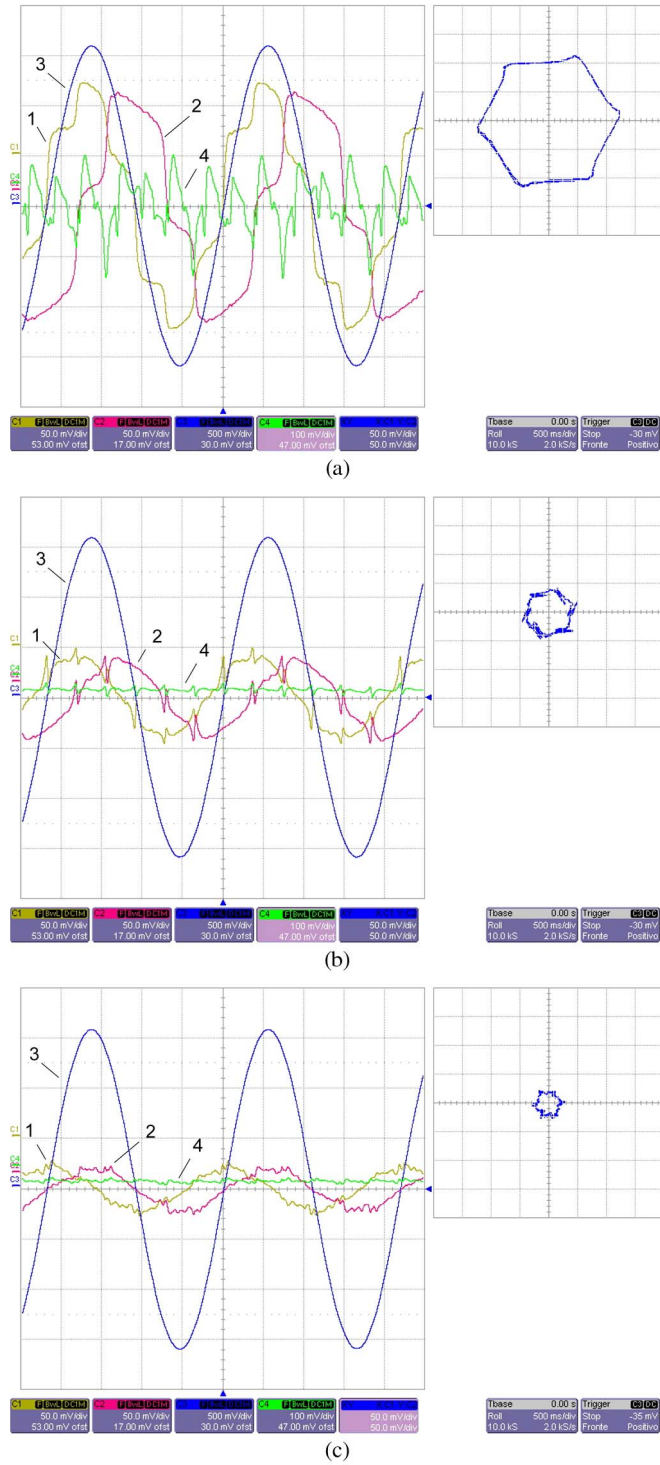


Fig. 8. Current control, open loop, no load, 25 r/min. Effect of the inverter error on the estimated back-EMF signals for different compensation situations. Scale factors: 500 ms/div, 1: $e_{s,\alpha}$ (4.5 V/div), 2: $e_{s,\beta}$ (4.5 V/div), 3: $i_{s,a}$ (0.7 A/div), 4: ω_e (180 r/min/div). (a) compensation OFF. (b) signum compensation. (c) LUT compensation.

To evaluate the field orientation accuracy, a sensed $VI\theta_r$ observer [18] operates parallel with the sensorless observer. The rotor flux position estimated by the sensed $VI\theta_r$ is compared with the one given by the sensorless observer that is used for field orientation. The results obtained for step-load transients are shown in Fig. 10. When signum compensation is used,

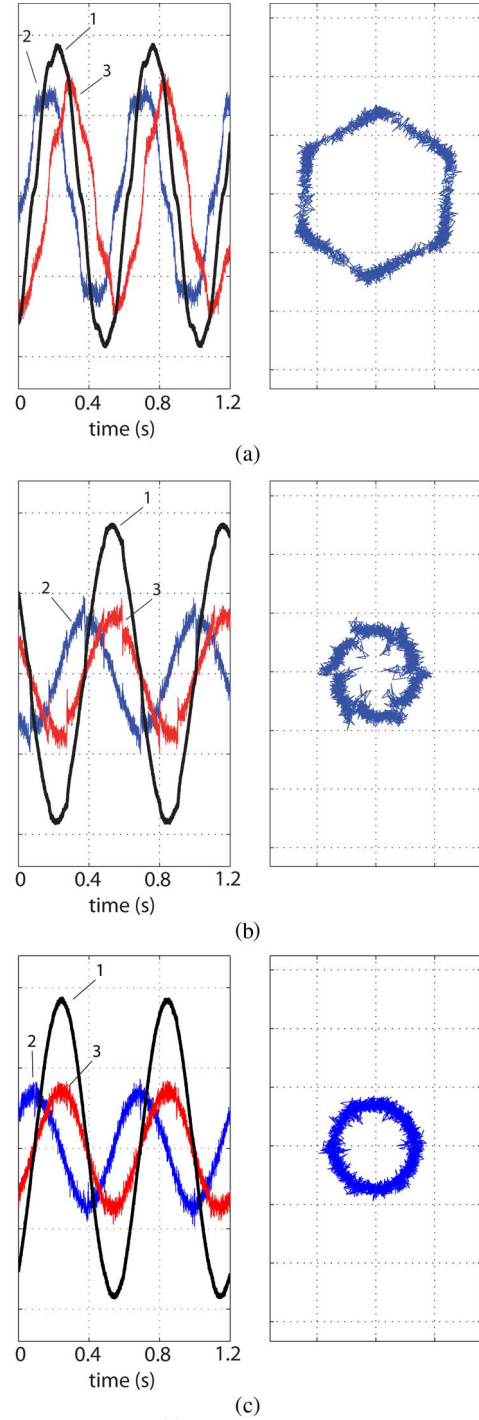


Fig. 9. SFOC, no load, 100 r/min. Effect of the inverter error on the estimated back-EMF signals for different compensation situations. Scale factors: 1: $i_{s,\alpha}$ (1.67 A/div), 2: $e_{s,\alpha}$ (5 V/div), 3: $e_{s,\beta}$ (5 V/div). XY plot: $e_{s,\alpha,\beta}$ (5 V/div). (a) compensation OFF. (b) signum compensation. (c) LUT compensation.

a slight orientation error occurs and the estimated speed is noisy and also the q -axis reference current. On the contrary, the LUT compensation exhibit better results: the estimated speed is much smoother, as is the q -axis reference current. The orientation error is better evidenced for the sensorless observed flux by representing in the top right subplots of Fig. 10 the flux components in the (d, q) synchronous reference frame defined by the sensed observed rotor flux vector. If no orientation

error exists, then the q -component of the sensorless flux is zero, as shown in Fig. 10(c) for LUT compensation. On the contrary, with signum compensation, the observed flux q -axis component is not zero, as shown in Fig. 10(b), while with no dead-time compensation, the orientation error is high [Fig. 10(a)]. Since the LUT is identified with dc current values, poor behavior may be expected during fast current transients. As shown in Fig. 10(c), the compensation performance is satisfactory when a step torque disturbance is applied to the motor. The current variation due to the load disturbance (1.5 A in 20 ms in the figure) is slow with respect to the 100 μ s PWM period and the LUT correctly compensates the average voltage error according to the average measured currents, as in dc conditions. A faster current variation can occur in case of a step reference torque and in this case, two opposite situations can be evidenced: a fast current controller would set a significant voltage reference in order to produce the requested current step, while a slow current controller would produce a slow current response. In the former case, the transient error of the LUT compensation during the fast current variation is not significant because the motor voltage is high during the transient. In the latter case, the current slope does not lead to a significant variation in the PWM period and the LUT compensation is correct.

The eventual variation of the dc-link voltage with respect to the LUT identification conditions would lead to an imprecise LUT compensation. The dc-link of the drive under test is largely variable with the motor load due to the single-phase passive rectifier input stage: the dc voltage drops in motoring and rises in regeneration up to the trigger level of the braking chopper. In the tests, the LUT has been identified at no load (305 V) and the minimum and maximum values at full load are 280 V and 330 V, respectively. However, significant dc-link variations are generated by a significant power flow, either absorbed or regenerated by the motor drive. At zero and around zero speed, which include the identification conditions and low speed operation (Figs. 10 and 11), there is nearly no power request and thus no dc-link variation. Even for high torque values, when the speed is low, the managed power is also low and the dc-link remains constant.

The performance of SFOC using the LUT compensation scheme was also evaluated by loading the IM with a synchronous machine with concentrated coils and an unskewed rotor. As a result, the load torque has high torque ripple content, as shown in Fig. 11. In spite of the load torque ripple, the IM is well controlled.

D. Sensorless Control, and Transition Between LUT and Signum Compensation

The motor is speed controlled using SFOC and the inverter compensation is suddenly changed from LUT to signum approach. The results are shown in Fig. 12 for two different motor speed values. The first transition is performed at 100 r/min and the results are shown in Fig. 12(a). It can be noted that the phase currents become distorted when the signum compensation is engaged; that is due to the speed loop that receives as feedback a distorted estimated speed. The difference between the LUT and the signum compensation schemes is more evident when

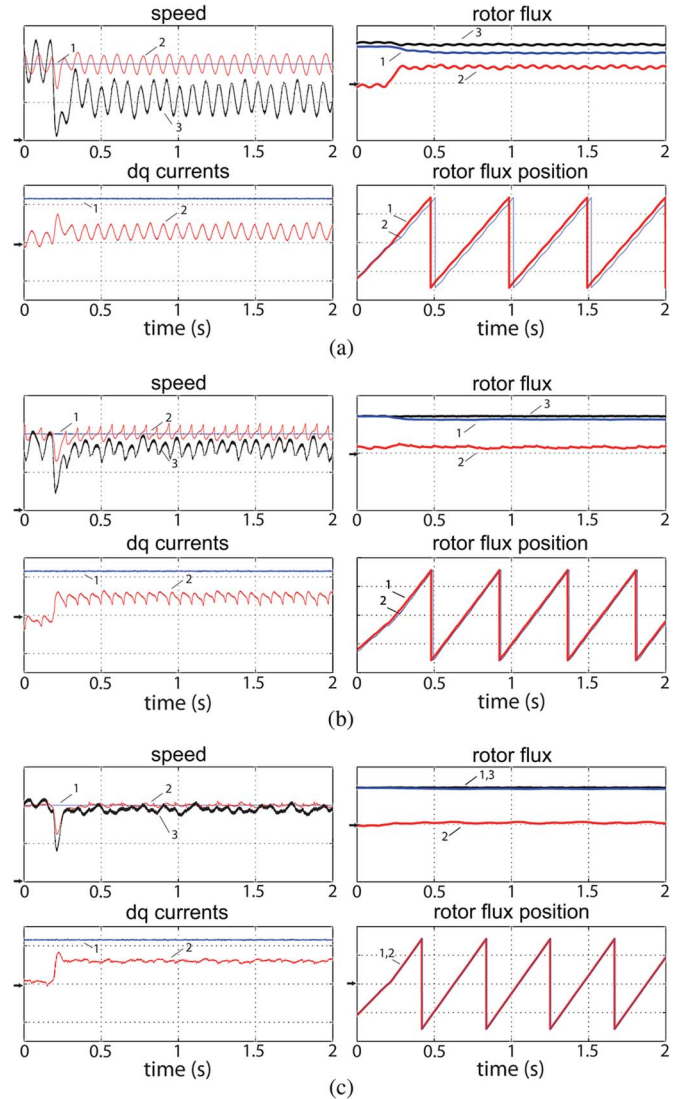


Fig. 10. SFOC, 100 r/min, load step. Effect of the inverter error on the estimated back-EMF signals for different compensation situations. Top left: 50 r/min/div. 1: reference speed, 2: estimated speed, 3: measured speed. Bottom left: 2 A/div. 1: $i_{s,d}$, 2: $i_{s,q}$. Top right: 0.25 Vs/div. 1: $\lambda_{r,d}$, 2: $\lambda_{r,q}$, 3: $|\lambda_r|$ is the sensorless observed flux in sensed observed coordinates. Bottom right: 2 rad/div. 1: rotor flux angle, sensorless, 2: rotor flux angle, sensed. (a) compensation OFF. (b) signum compensation. (c) LUT compensation.

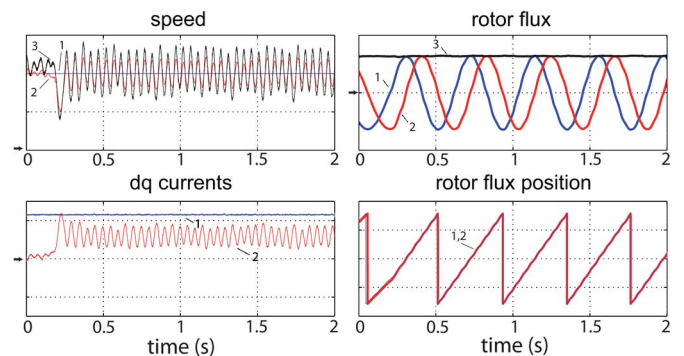


Fig. 11. SFOC, 100 r/min, load step with torque ripple. The torque of the loading machine presents a 12th harmonic ripple. Top left: 50 r/min/div. 1: reference speed, 2: estimated speed, 3: measured speed. Bottom left: 2 A/div. 1: $i_{s,d}$, 2: $i_{s,q}$. Top right: 0.25 Vs/div. 1: $\lambda_{r,\alpha}$, 2: $\lambda_{r,\beta}$, 3: $|\lambda_r|$. Bottom right: 2 rad/div. 1: rotor flux angle, sensorless, 2: rotor flux angle, sensed.

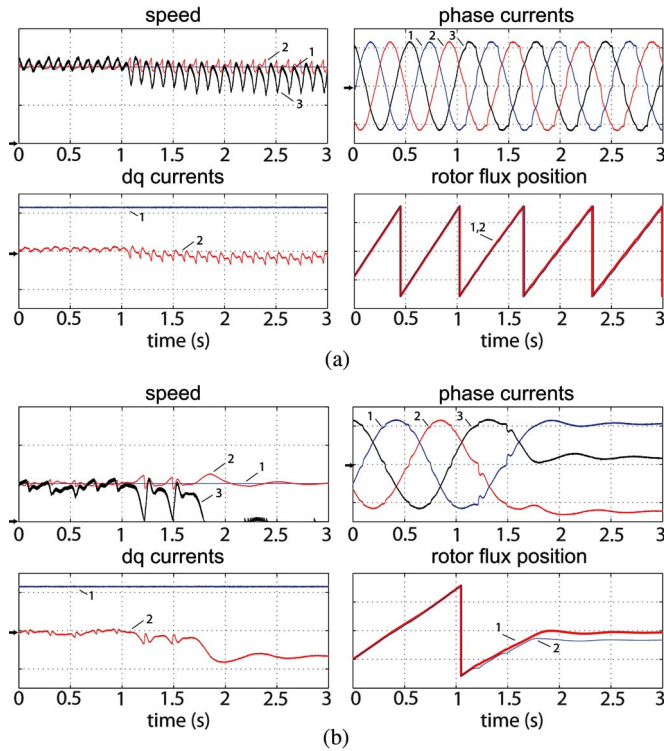


Fig. 12. SFOC, effect of the transition from LUT compensation to signum compensation at 50 r/min and 100 r/min. Top left: 50 r/min/div. 1: reference speed, 2: estimated speed, 3: measured speed. Bottom left: 2 A/div. 1: $i_{s,d}$, 2: $i_{s,q}$. Top right: 2 A/div. 1: $i_{s,a}$, 2: $i_{s,b}$, 3: $i_{s,c}$. Bottom right: 2 rad/div. 1: rotor flux angle, sensorless, 2: rotor flux angle, sensed. (a) 100 r/min. (b) 50 r/min.

the motor is running at 50 r/min at no load when the signum compensation is engaged, as shown in Fig. 12(b). In fact, the SFOC using the signum compensation loses control and the motor stops completely. The same two tests are repeated with the dead-time set to 2 μ s and relative LUT compensation in Fig. 13. Similar results are obtained, even if a residual distortion is evidenced on the estimated speed and on the phase currents also with LUT compensation. A possible solution for reducing the residual distortion is to augment the number of points of the LUT (e.g., 64 points LUT instead of 32 points) in order to better represent the back-EMF error at very low current values (phase current < 0.25 A).

V. CONCLUSION

This paper has presented a new technique for the compensation of the inverter nonlinear effects in SFOC IM drives. The compensation technique is more accurate than the signum-model-based ones and at the same time, it is very simple to implement. The inverter model is identified directly by the digital controller at the drive startup with no extra hardware and no extra measures. No additional processing or tuning are required after the commissioning session. The inverter identification is performed by means of the feedback signal of the flux observer, which must include closed-loop back-EMF integration. The method allows the stator resistance, including the on-state drops, to be obtained. A comprehensive set of experimental results has been presented for a rotor-flux-oriented sensorless IM drive for home appliance in order to demonstrate the feasibility of the proposed solution.

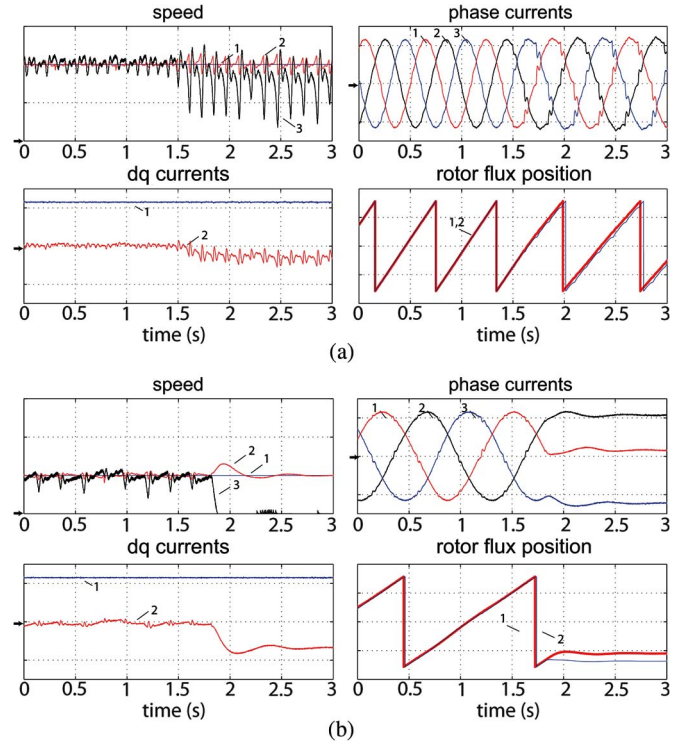


Fig. 13. SFOC, effect of the transition from LUT compensation to signum compensation at 50 r/min and 100 r/min but using a dead-time of 2 μ s. Top left: 50 r/min/div. 1: reference speed, 2: estimated speed, 3: measured speed. Bottom left: 2 A/div. 1: $i_{s,d}$, 2: $i_{s,q}$. Top right: 2 A/div. 1: $i_{s,a}$, 2: $i_{s,b}$, 3: $i_{s,c}$. Bottom right: 2 rad/div. 1: rotor flux angle, sensorless, 2: rotor flux angle, sensed. (a) 100 r/min. (b) 50 r/min.

APPENDIX

RATINGS OF THE EXPERIMENTAL SETUP

The motor under test is rated: 700 W, 195 V, 3 A, 2 poles, 17 000 r/min maximum speed. The inverter rating is: 220 V, 50 Hz single-phase input, passive rectifier. IGBT SOA: 600 V, 10 A. Dead-time setting is 1 μ s. The switching frequency is 10 kHz.

REFERENCES

- [1] J. Holtz, "Sensorless control of induction motor drives," *Proc. IEEE*, vol. 90, no. 8, pp. 1359–1394, Aug. 2002.
- [2] C. Schauder, "Adaptive speed identification for vector control of induction motors without rotational transducers," *IEEE Trans. Ind. Appl.*, vol. 28, no. 5, pp. 1054–1061, Sep./Oct. 1992.
- [3] S. Doki, S. Sangwongwanich, T. Yoenmoto, and S. Okuma, "Speed-sensorless field-oriented control using adaptive sliding mode observers," in *Conf. Rec. IEEE IECON*, 1990, pp. 453–458.
- [4] K. D. Hurst, T. G. Habetler, G. Griva, and F. Profumo, "Zero-speed tachless IM torque control: Simply a matter of stator voltage integration," *IEEE Trans. Ind. Appl.*, vol. 34, no. 4, pp. 790–795, Jul./Aug. 1998.
- [5] H. Kubota, K. Matsuse, and T. Nakano, "DSP-based speed adaptive flux observer of induction motor," *IEEE Trans. Ind. Appl.*, vol. 29, no. 2, pp. 344–348, Mar./Apr. 1993.
- [6] C. Lascu and G.-D. Andreescu, "Sliding-mode observer and improved integrator with dc-offset compensation for flux estimation in sensorless-controlled induction motors," *IEEE Trans. Ind. Electron.*, vol. 53, no. 3, pp. 785–794, Jun. 2006.
- [7] L. Harnefors, "Design and analysis of general rotor-flux-oriented vector control systems," *IEEE Trans. Ind. Electron.*, vol. 48, no. 2, pp. 383–390, Apr. 2001.
- [8] L. Harnefors and M. Hinkkanen, "Complete stability of reduced-order and full-order observers for sensorless IM drives," *IEEE Trans. Ind. Electron.*, vol. 55, no. 3, pp. 1319–1329, Mar. 2008.

- [9] J. Choi and S. Sul, "Inverter output voltage synthesis using novel dead time compensation," *IEEE Trans. Power Electron.*, vol. 11, no. 2, pp. 221–227, Mar. 1996.
- [10] R. Sepe and J. Lang, "Inverter nonlinearities and discrete-time vector current control," *IEEE Trans. Ind. Appl.*, vol. 30, no. 1, pp. 62–70, Jan./Feb. 1994.
- [11] J. K. Pedersen, F. Blaabjerg, J. W. Jensen, and P. Thogersen, "An ideal PWM-VSI inverter with feedforward and feedback compensation," in *Conf. Rec. EPE*, 1993, pp. 501–507.
- [12] J. Holtz and J. Quan, "Sensorless vector control of induction motors at very low speed using a nonlinear inverter model and parameter identification," *IEEE Trans. Ind. Appl.*, vol. 38, no. 4, pp. 1087–1095, Jul./Aug. 2002.
- [13] S. Bolognani and M. Zigliotto, "Self-commissioning compensation of inverter non-idealities for sensorless AC drives applications," in *Proc. IEE Power Electron., Mach. Drives*, 2002, pp. 30–37.
- [14] S. Bolognani, L. Peretti, and M. Zigliotto, "Repetitive-control-based self-commissioning procedure for inverter nonidealities compensation," *IEEE Trans. Ind. Appl.*, vol. 44, no. 5, pp. 1587–1596, Sep./Oct. 2008.
- [15] J. Guerrero, M. Leetmaa, F. Briz, A. Zamarron, and R. Lorenz, "Inverter nonlinearity effects in high-frequency signal-injection-based sensorless control methods," *IEEE Trans. Ind. Appl.*, vol. 41, no. 2, pp. 618–626, Mar./Apr. 2005.
- [16] G. Pellegrino, P. Guglielmi, E. Armando, and I. Bojoi, "Self-commissioning algorithm for inverter non-linearity compensation in sensorless induction motor drives," in *Conf. Rec. 43rd IEEE IAS Annu. Meeting*, Oct. 2008, pp. 1–7.
- [17] G. Pellegrino, R. Bojoi, and P. Guglielmi, "Performance comparison of sensorless field oriented control techniques for low cost three-phase induction motor drives," in *Conf. Rec. 42nd IEEE IAS Annu. Meeting*, Sep. 2007, pp. 281–288.
- [18] P. Jansen and R. Lorenz, "A physically insightful approach to the design and accuracy assessment of flux observers for field oriented induction machine drives," *IEEE Trans. Ind. Appl.*, vol. 30, no. 1, pp. 101–110, Jan./Feb. 1994.



Gianmario Pellegrino (M'06) received the M.Sc. and Ph.D. degrees in electrical engineering from the Politecnico di Torino, Turin, Italy, in 1998 and 2002, respectively.

Since 2002, he has been with the Department of Electrical Engineering, Politecnico di Torino, first as a Research Associate and then as an Assistant Professor. He has been teaching courses on power electronics and electric drives since 2007. He is involved in research projects for the public sector and for private groups, and he has written more than 30 technical papers. He also holds one international patent. His areas of interest include electric drives, particularly in motor design and digital control. He works in the fields of electric traction and in the design of direct-drive generators for wind energy production. He was a Guest Researcher at Aalborg University, Aalborg, Denmark, in 2002.



Radu Justin Bojoi (M'06) received the M.Sc. degree in electrical engineering from the Technical University "Gh. Asachi" Iasi, Romania, in 1993, and the Ph.D. degree from Politecnico di Torino, Turin, Italy, in 2003.

From 1994 to 1999, he was an Assistant Professor in the Department of Electrical Drives and Industrial Automation of the Technical University of Iasi. In 2004, he joined the Department of Electrical Engineering of the Politecnico di Torino as an Assistant Professor. His scientific interests include the design and development of DSP- and FPGA-based advanced control systems in the fields of power electronics, high-performance electrical drives, and power-conditioning systems. He has published more than 60 papers in international conference proceedings and technical journals.

Dr. Bojoi received the IPEC First Prize Paper Award in 2005.



Paolo Guglielmi (M'07) was born in Imperia, Italy, in 1970. He received the M.Sc. degree in electronic engineering and the Ph.D. degree in electrical engineering from the Politecnico di Torino, Turin, Italy, in 1996 and 2001, respectively.

In 1997, he joined the Department of Electrical Engineering, Politecnico di Torino, where he became a Researcher in 2002. He has authored several papers published in technical journals and conference proceedings. His fields of interest include power electronics, high-performance servo-drives, and computer-aided design of electrical machines.

Dr. Guglielmi is a Registered Professional Engineer in Italy.



Francesco Cupertino (M'08) was born on December 1972. He received the Laurea degree and the Ph.D. degree in electrical engineering from the Technical University of Bari, Bari, Italy, in 1997 and 2001, respectively.

From 1999 to 2000, he was with the PEMC research group, University of Nottingham, Nottingham, U.K. Since July 2002, he has been an Assistant Professor in the Electrical and Electronic Engineering Department of the Technical University of Bari, where he teaches two courses on electrical drives. His research interests include intelligent motion control of electrical machines, applications of computational intelligence to control, sliding-mode control, sensorless control of ac electric drives, signal processing techniques for three-phase signal analysis, and fault diagnosis of ac motors. He is the author or coauthor of more than 70 scientific papers on these topics.

Dr. Cupertino is a Registered Professional Engineer in Italy.